Passive guided wave tomography for erosion monitoring in an air/sand test loop

Tom Druet, Axel Thomas, Arnaud Recoquillay, Bastien Chapuis

Passive Guided Wave Tomography for Erosion Monitoring in an Air/Sand Test Loop

Tom Druet[1], Axel Thomas[1], Arnaud Recoquillay[1], and Bastien Chapuis[1]

[1] Université Paris-Saclay, CEA, List, F-91120, Palaiseau, France

*corresponding author, E-mail: tom.druet@cea.fr

Abstract

The detection and quantification of defects in pipes by non-destructive testing techniques plays a crucial role in several industries (petrochemical and nuclear in particular). Once a defect is detected, assessing its severity enables to schedule maintenance appropriately, hence reducing maintenance cost and rupture or leakage risks.

Structural Health Monitoring (SHM) is an approach that consists in instrumenting a structure with permanent sensors to monitor its health status throughout its life. Guided elastic waves are particularly suitable for SHM applications on thin structures (such as pipes) thanks to their ability to propagate over long distances and their high sensitivity.

An SHM approach called "passive guided waves tomography" has emerged in recent years to detect and quantify corrosion in pipes (or plate-like structures). This technology is based on the combination of guided elastic wave tomography algorithms and a passive method such as the so-called ambient noise cross-correlation. It allows to obtain absolute and precise maps of the thickness of an area surrounded by a distribution of sensors without emitting waves, simply by analyzing the elastic noise that exists naturally in the pipe (due to vibrations, fluid-structure interactions with a moving fluid, etc.).

In this paper passive guided waves tomography is tested in representative conditions thanks to an erosion loop that circulates air and sand. By impacting the tube wall, sand grains erode the structure, creating thickness losses that we monitor with passive tomography.

1. Introduction

Guided elastic waves are promising tools for nondestructive testing: they are waves propagating over large distances due to the geometry of the structure [1]. They can be used in many cases such as plate-like [2], pipe-like [3,4] or rail-like structures [5], enabling to inspect a large area in a single acquisition and thus limiting the needed time or number of sensors. Guided waves are particularly interesting in the context of Structural Health Monitoring (SHM), for which the intrusiveness of the system may be a very important factor to be taken into account (added mass, complexity to be deployed, etc.).

Pipelines in particular are a subject of interest for SHM as they are used in many industrial applications such as the oil&gas industry or nuclear power plants, and their safety is of utmost importance to avoid any spillage, which may have dramatic ecological, social and economic consequences. Pipelines are enduring erosion or corrosion which will induce a loss of thickness. By monitoring the residual thickness with a good accuracy, it is hence possible to prevent leakage, but also to plan the maintenance to limit as much as possible the down time, thus optimizing the costs.

The method shown in this paper, the so-called guided waves tomography [6,7], enables the reconstruction of a residual thickness map of the structure. It can be used for NDT but also for SHM as an autocalibration procedure allows to determine the absolute residual thickness map [8]. This approach makes it less sensitive to Environmental and Operational Conditions (EOCs) such as the temperature [9]. In this context, it is needed that the method works while the structure itself is operating, inducing noise in the measurements. To circumvent this difficulty, we propose to use a passive method called “ambient noise cross-correlation” [10,11,12,13]. This method uses the ambient elastic noise to recover equivalent data to the ones obtained in a classic active framework where transducers are used to emit waves in the structure. In passive approach, no excitation is needed, which enables the use of sensors only measuring waves such as Fiber Bragg Gratings (FBG) [13,14]. A work started on the use of FBGs to perform guided wave tomography and more specifically on the effect of FBG receivers’ directivity on this imaging method [15].

We show in this paper an application of the method to a representative test case: a pipe was instrumented in an accelerated air/sand erosion test loop. The noise from the test itself was used as our input data to reconstruct the evolution of the residual thickness of the instrumented part, this residual thickness evolving during the test.

In a first part, the main aspects of the method are recalled, before presenting with more details in a second part the test case and the corresponding results.

2. Description of the Technique

We first present the method, which can be decomposed in two main parts: the guided wave tomography algorithm, which is an imaging method suited for the quantitative

imaging of waveguide structures such as plates or pipes, and passive techniques, which enable the reconstruction of equivalent signals to classic active acquisitions.

2.1. Guided wave tomography

Guided wave tomography algorithms are based on a single mode assumption, which enables to link an information extracted from the signals to the residual thickness of the structure thanks to the dispersion curves of the mode. This information can either be a time of flight, for time of flight tomography methods, linking the group or energy velocity to the residual thickness, or a phase, for diffraction tomography methods, linking the phase velocity to the residual thickness. We consider here diffraction tomography (DT) detailed in [8] and initially inspired by [6]. Note that DT is used here instead of iterative DT because the thickness losses due to sand erosion are quite weak which implies that Born approximation is respected but the results would be roughly the same with iterative DT. The DT method is based on the Lippmann-Schwinger equation: for an emitter located at point $\boldsymbol{i}$ and a receiver located at point $\boldsymbol{j}$, the measured scattered field $\boldsymbol{\varphi^s(x_j, x_i)}$ at a given frequency $\boldsymbol{\omega}$ can be written as

$$\boldsymbol{\varphi^s(x_j, x_i) = \int G_0(x_j, x) O(x) \varphi_0(x, x_i) dx}, \quad (1)$$

Where $\boldsymbol{G_0}$ is the Green's function of the Helmholtz equation in the current domain $\boldsymbol{\Omega}$, $\boldsymbol{\varphi_0}$ is the unperturbed field and $\boldsymbol{O(x) = k^2(x) - k_0^2}$ is the object function, where $\boldsymbol{k}$ is the wave number and $\boldsymbol{k_0}$ is the wave number for the nominal thickness. By inverting the Lippmann-Schwinger equation, the object function can be updated to reconstruct the residual thickness, once again through the dispersion curves linking the wave number to the thickness.

To compensate for model errors, an autocalibration method is used [8]. This method makes the technique completely baseline free and allows to estimate the absolute thickness of the structure instead of a relative thickness when a baseline is used. The idea is, for all couples, to compute a calibration factor by which the data will be multiplied in order to compensate the gap between model and data. All the potential autocalibration factors are computed as

$$\boldsymbol{c_{ij} = \frac{G_0(x_j, x_i)}{\varphi(x_j, x_i)}}, \quad (2)$$

Where $\boldsymbol{\varphi}$ is the total field. As some of the paths of the couples will cross some defect, a confidence ellipse is used to keep only the factors corresponding to healthy paths to perform the autocalibration of the tomography data. Indeed, the mean of all the factors corresponding to healthy paths is used to calibrate all the data.

2.2. Passive data

Contrary to classic active data acquisitions, as described in the previous section, passive data do not rely on sensors emitting waves. Indeed, it can be proved in the case of diffuse fields [11] that equivalent data to active signals can be recovered. Let $\boldsymbol{\varphi_i}$ and $\boldsymbol{\varphi_j}$ be the ambient noise measured by sensors $\boldsymbol{i}$ and $\boldsymbol{j}$ and let $\boldsymbol{C(x_j, x_i, t; T)}$ be their cross-correlation over the time window (0,T). It can be shown that

$$\boldsymbol{\lim_{T \to +\infty} \frac{\partial C}{\partial t}(x_j, x_i, t; T) \propto F * [\varphi(x_j, x_i, \cdot) - \varphi(x_j, x_i, -\cdot)](t)}, \quad (3)$$

Where $\boldsymbol{F}$ is linked to the spectral density of the ambient noise. We hence retrieve the impulse response of the system, as if one of the sensors was an emitter, for a bandwidth linked to the one of the ambient noise.

In this paper the diffuse field also called ambient elastic noise is due to the impact of the sand on the tube wall.

3. Results

In this paper, the passive guided wave tomography technique is tested on an erosion loop to represent as much as possible the reality. This section describes first the experimental setup and then tomography images as the erosion due to the sand flow increases are presented for active and passive data.

3.1. Experimental setup

The instrumented structure is a stainless steel pipe with a flange at each end and with an elbow and a straight part. The nominal healthy thickness of the wall is 7.3mm and the theoretical outer diameter is 143.1mm. Note that it is well known that depending on how the tube is manufactured, the tolerance on the thickness can reach 15% of the theoretical wall thickness. Both the bended part and the straight part were instrumented with fiber Bragg gratings (FBG) and piezoelectric transducers (PZT) but this paper focuses on the straight part instrumented with PZTs. Indeed, two rings of 16 PZTs were bounded to the pipe using epoxy glue as shown in Figure 1.

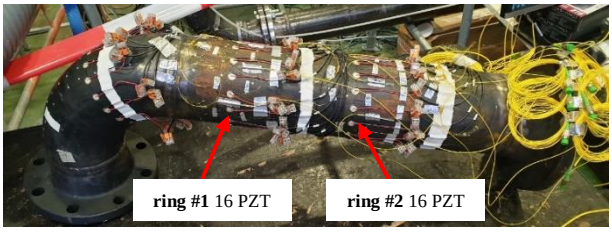

Figure 1: The studied structure instrumented with two rings of PZTs.

This piece was mounted at the end of the erosion loop thanks to the flanges just before a flexible pipe used for sand exhaust as shown in Figure 2.

The tests lasted one week. During this week 6 batches of 700 kg of sand each were poured into the test loop thanks to a vessel also shown in Figure 2. One batch testing took 3 hours. Post-mortem punctual US measurements were performed to get a reference of the thickness loss in the inspected area for one batch of sand. The maximal thickness loss average is around 0.08mm per batch.

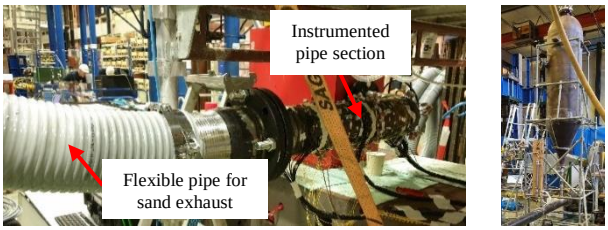

Figure 2: The studied structure is mounted to the erosion loop (left) and the sand vessel (right).

Finally, one PT100 sensor has been attached to the section under test in order to get its surface temperature during the week. The evolution of the temperature is shown in Figure 3. We can see on this figure that when the erosion loop is working the temperature increases quickly due to the multiple sand grains impacting the pipe wall. The increase is of about 30°C until a temperature stage that is between 37°C and 39°C. During the night the temperature is decreasing to the ambient temperature of the room.
The PZT measurement process was fully automated, and switched regularly between passive and active measurements, during each batch.

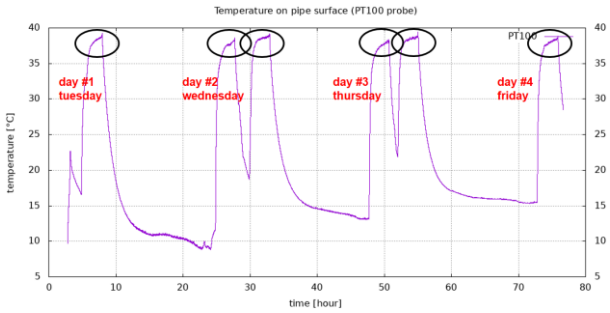

Figure 3: Temperature given by the PT100 probe on the surface of the pipe during the week of tests.

3.2. Signal processing

As explained before, PZT sensors were used both in active mode and passive mode and that during all the batches. We recall that:

- In active mode, the acoustic signals are measured in transmission between all the couples of sensors. Each sensor is excited successively and the elastic guided waves are measured by all the other sensors.
- In passive mode, there is no emission of wave, all sensors measure the ambient noise generated by the sand impacts during a long time. The ambient noise is then post-processed thanks to the passive method presented before which is able to reconstruct the same signals than the ones obtained in active mode.

3.2.1. Active signals

Regarding the active acquisition, a Hann burst of 5 cycles was used for multiple center frequencies. In this paper, only frequency 90 kHz is used. For this structure, the corresponding wavelength is about 22.5mm for the L(0, 1) mode (equivalent to A0 in plates). The signals measured with all the sensors for an emission with PZT #8 in the pristine state are presented in Figure 4. The signal in dashed line corresponds to the emitter. The electromagnetic coupling is clearly identified between 0µs and 50µs and then wave packets corresponding to the direct and helical modes are visible.

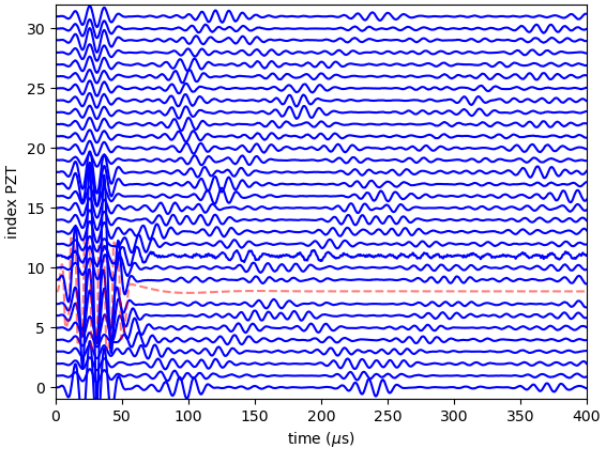

Figure 4: Signals for an emission with PZT #8 before the erosion loop starts.

When the erosion loop is started, it is generating ambient noise (from electromagnetic and mechanical sources) that is measured by the sensors and the acquisition system as we can see in Figure 5.

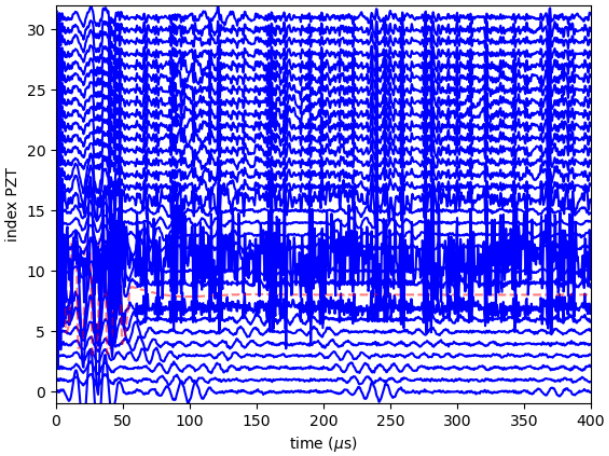

Figure 5: Signals for an emission with PZT #8 after the erosion loop starts.

By filtering and averaging, it is possible to obtain signals of better quality, see Figure 6. The ambient noise degrades the quality of the data when the loop is in operation which is a disadvantage of active methods. In that case, it can be interesting to work with passive measurements as discussed in the next section.

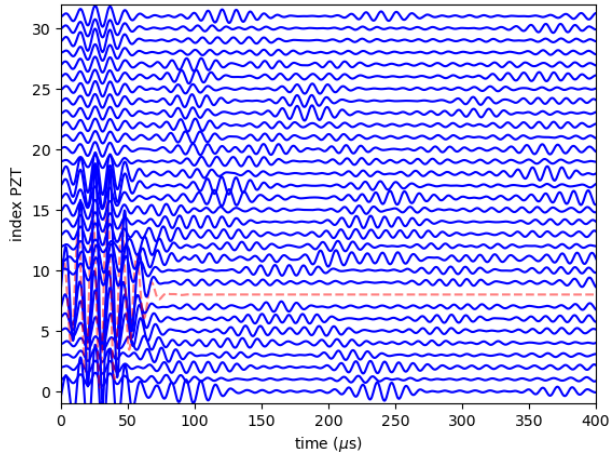

Figure 6: Signals for an emission with PZT #8 after the erosion loop starts and with filtering and averaging.

3.2.2. Passive signals

As far as the passive acquisition is concerned, 20s of ambient noise is measured by all the sensors. A portion of 1ms is presented in Figure 7. High energy signatures are visible in the figure. They are synchronized in time for all sensors. This mean that the origin is electromagnetic. The mechanical ambient noise that is used to obtain the Green functions is of smaller energy.

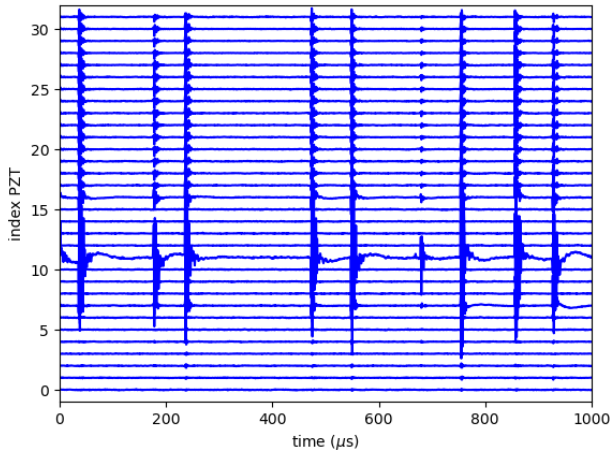

Figure 7: Small portion of the ambient noise measured by all the sensors when the erosion loop is in operation.

To convince ourselves that the synchronized events are due to the test loop in operation, the same portion of noise are plotted in Figure 8 when the loop is out of operation. The signals have been normalized in this figure because the energy measured was several order of magnitude bellow. The events are not visible in this figure, we can only see electronic noise.

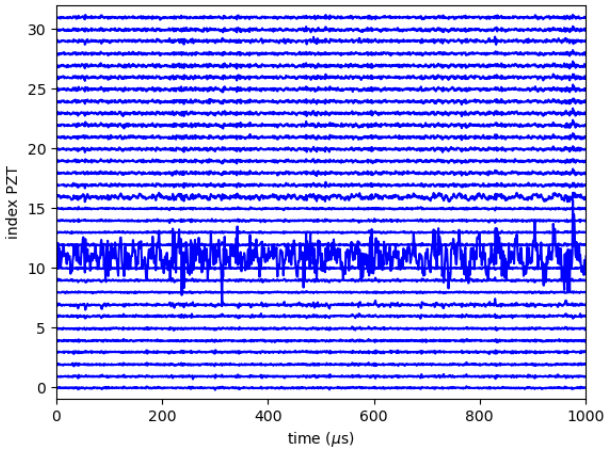

Figure 8: Small portion of the ambient noise measured by all the sensors when the erosion loop is out of operation.

Then, acquired ambient noise in operation is processed with the passive method presented above to obtain the passive signals. An example of obtained passive signals is presented in Figure 9.

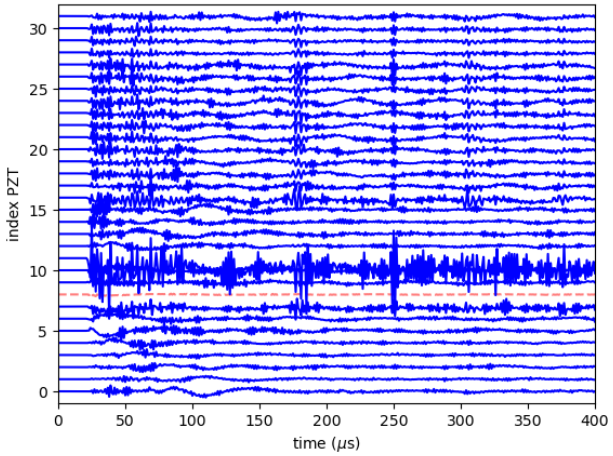

Figure 9: Passive signals as if PZT #8 is emitter. The erosion loop is in operation.

Finally, a band-pass filter centered to 90 kHz, and having the same spectrum as the Hann burst used in active, is used to get signals comparable with active signals, see Figure 10. The quality of those signals is quite good: the correlation residuals, that is wave packets not corresponding to physical waves which come from the processing, are of small amplitude when compared to the physical wave packets we want to recover. It means that a good convergence toward the Green's functions has been achieved for this acquisition length. Note finally that, compared to active signals, the time-of-flights of the wave packets of interest are shifted of half the duration of the active signal Hann burst due to the fact that in active the time vector starts at the beginning of the emission of the Hann burst.

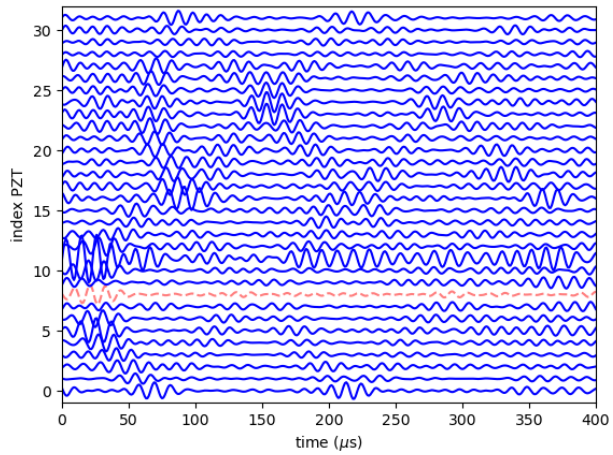

Figure 10: Filtered passive signals as if PZT #8 is emitter. The erosion loop is in operation.

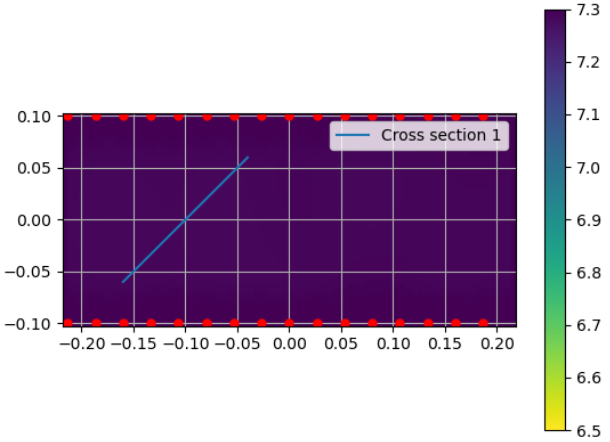

Figure 11: Relative active tomography with a baseline at 37°C and computed at the start of the test. The colorbar is in millimeters and the axes are in meters.

3.3. Thickness reconstruction by guided wave tomography

In that last section of results are presented active and passive guided wave tomography images using the signals of last section as data.

3.3.1. Active tomography for relative reconstructions

Active tomography using a baseline is firstly presented in this subsection. In order to avoid as much as possible the effect of temperature variations, the baseline used is the first measurement in day#1 just after the temperature reaches the stage around 37°C (see Figure 3). This choice is mainly done because it is known that if a shift in environmental conditions exist between the baseline and the current signals, this will imply a bias, or, in the worst case, this can cause very bad reconstructions of the potential defects as the properties of the guided modes such as phase or energy velocity may change significantly. All the images and cross sections of this section are computed using the data measured when the stage around 37°C/39°C is achieved. This corresponds to the black circles in Figure 3.

The first image of relative active tomography computed with signals measured just after the test started is presented in Figure 11. Note that in this image and the following ones, an unrolled view of the pipe is shown, the red dots representing the sensors along the circumference. As it is relative tomography, no thickness losses are visible in the image which is coherent because the sand grains did not have the time to erode the structure yet.

The final image of relative tomography computed with signals measured at the end of the test is presented in Figure 12. This time, a loss of thickness is reconstructed by the relative tomography. The position of the erosion is coherent with the theoretical impact zone of sand grains coming from the elbow outlet. Moreover, the path is expected to be slightly off the pipe axis which is also coherent with the tomography image.

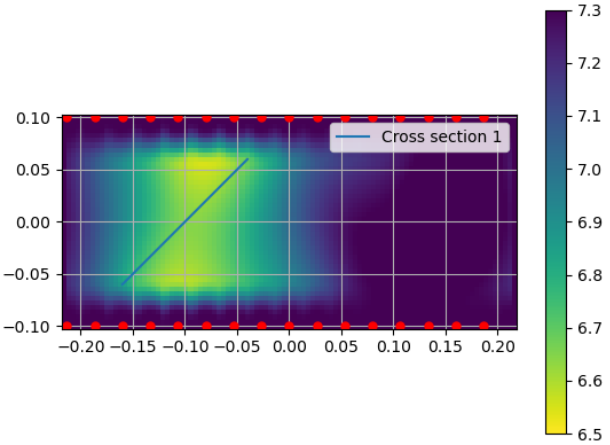

Figure 12: Relative active tomography with a baseline at 37°C and computed at the end of the test. The colorbar is in millimeters and the axes are in meters.

Regarding the loss of thickness due to the erosion, the cross section corresponding to the blue line in the images is plotted in Figure 13 for all the tomography images computed during the erosion test. The bluer the curve, the closer to the beginning of the erosion test the data were acquired and the redder the curve, the closer to the end of the test were the data acquired. As discussed before, punctual US measurements were performed during the erosion test. This allows to estimate the maximal thickness loss with a method of reference. With this method, the global maximal thickness

loss was estimated at 0.51mm +/- 0.1mm. Figure 13 shows a maximal thickness loss of 0.65mm which is a good estimate compared to the punctual US measurements despite the fact that the dispersion curves used to compute the tomography images were computed for the ambient temperature.

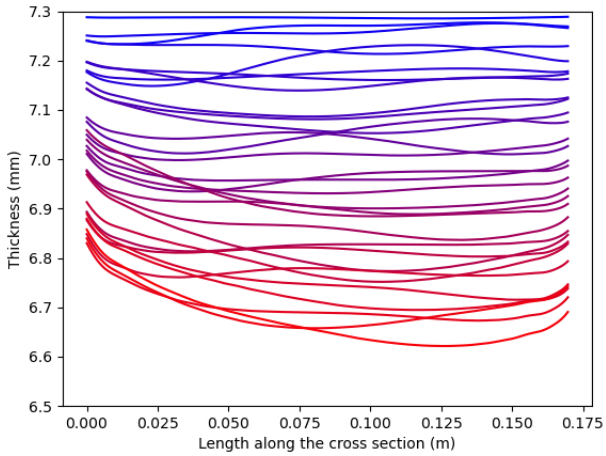

Figure 13: Cross sections of all relative active tomography images (with a baseline at 37°C) computed during the erosion test.

In order to be more realistic on the use of a baseline, the same study is performed but with a baseline measured at ambient temperature (10°C, see Figure 3) just before the test starts. The same data at high temperature, i.e. between 37°C and 39°C, are used to compute all the images. The image computed at the start of the test is presented in Figure 14. Comparing this figure to Figure 11 we can see thickness losses when there should not be any. This is due to the difference of temperature between the baseline and the current state, leading to artifacts in the image.

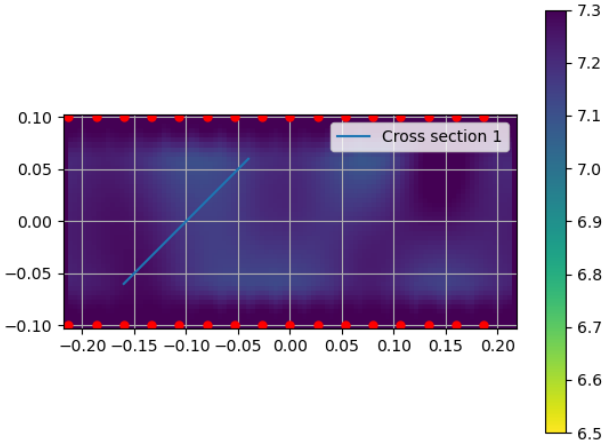

Figure 14: Relative active tomography with a baseline at ambient temperature (10°C) and computed at the start of the test. The colorbar is in millimeters and the axes are in meters.

Regarding the image computed at the end of the test, it is presented in Figure 15. Once again, Comparing this figure to Figure 12 we can clearly see that the estimated thickness losses are higher because of the difference of temperature between the baseline and the current state.

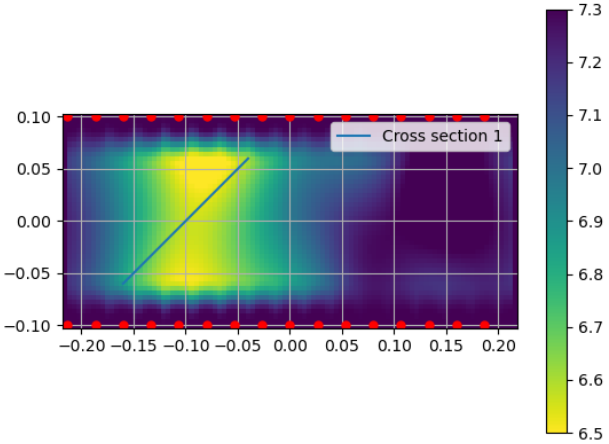

Figure 15: Relative active tomography with a baseline at ambient temperature (10°C) and computed at the end of the test. The colorbar is in millimeters and the axes are in meters.

We finally present in Figure 16 all the cross sections of images for the realistic baseline measured at ambient temperature (10°C). It is found that, comparing to Figure 13, the final estimation of the maximal thickness loss is overestimated by 0.1mm. Indeed, it shows a maximal thickness loss of about 0.75mm whereas Figure 13 shows a maximal thickness loss of about 0.65mm. We recall that punctual US measurements estimated a maximal thickness loss of 0.51mm +/- 0.1mm. This shows that the use of a baseline can introduce a bias in guided wave tomography.

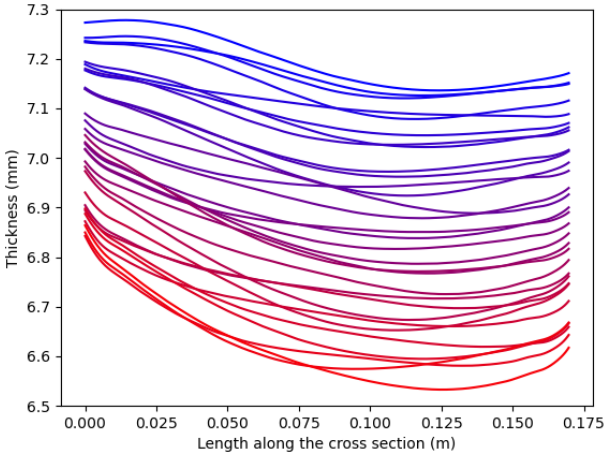

Figure 16: Cross sections of all relative active tomography images (with a baseline at 10°C) computed during the erosion test.

This study demonstrates that a baseline can become obsolete if it is not coherent with the environmental conditions of the current state. For guided wave tomography it introduces a bias, but for other guided waves processing methods it can

lead to very bad results if the changes of environmental conditions are not modeled correctly. This is one of the reason why we prefer to work in absolute with the use of the autocalibration method in an SHM framework. Absolute tomography is studied in the two following subsections.

3.3.2. Active tomography for absolute reconstructions

In this subsection is studied baseline free active tomography. This allows to compute absolute reconstructions of the wall thickness in the inspected area. Absolute tomography is made possible thanks to the autocalibration method recalled in the previous section.
The first image of absolute tomography computed with signals measured just after the test started is presented in Figure 17. Unlike relative tomography results, here, in absolute tomography, the thickness background is not uniform even if no erosion is created by the sand yet. This is probably because the wall thickness of the pipe is not constant because of the manufacturing process. As mentioned before, the tolerance on the thickness can reach 15% of the theoretical wall thickness meaning that for the structure of interest in this paper, the healthy thickness can vary from 6.2mm to 8.4mm, that is not negligible. Thus, absolute tomography appears to be a very attractive method compared to relative tomography to assess the real remaining thickness of the structure, which is the critical parameter to estimate the pipe health. It should be noted that we were unable to prove rigorously on these tests that the absotute tomography image in Figure 17 corresponds precisely to variations in the absolute thickness of the pipe, as we did not performed punctual US measurements over the entire inspection area.

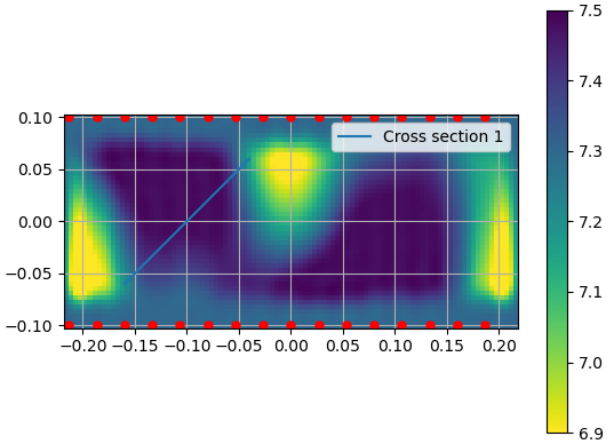

Figure 17: Absolute active tomography computed at the start of the test. The colorbar is in millimeters and the axes are in meters.

The absolute tomography computed at the end of the test is presented in Figure 18. By comparing to Figure 17, it shows a thickness reduction in the left part of the image. This reduction is once again coherent with the erosion by the impacts of the sand grains.

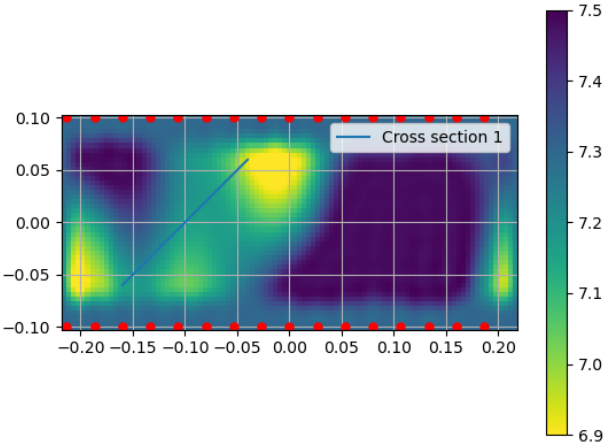

Figure 18: Absolute active tomography computed at the end of the test. The colorbar is in millimeters and the axes are in meters.

To estimate the quality of the estimation of thickness losses, cross sections are plotted in Figure 19. The cross sections are substantially different from the ones of relative tomography in Figure 13. Indeed, relative tomography assumes that the healthy thickness is constant whereas absolute tomography is able to reconstruct the absolute thickness. Figure 19 shows a maximal thickness loss of 0.4mm which is a good estimation even if it is slightly underestimated compared to the punctual US measurements that give 0.51mm +/- 0.1mm. We recall that the precision of guided wave tomography on the thickness estimation is around 0.1mm. This confirms that the results on Figure 19 are of good quality. Recall that the used dispersion curves were computed for an ambient temperature, inducing a model error.

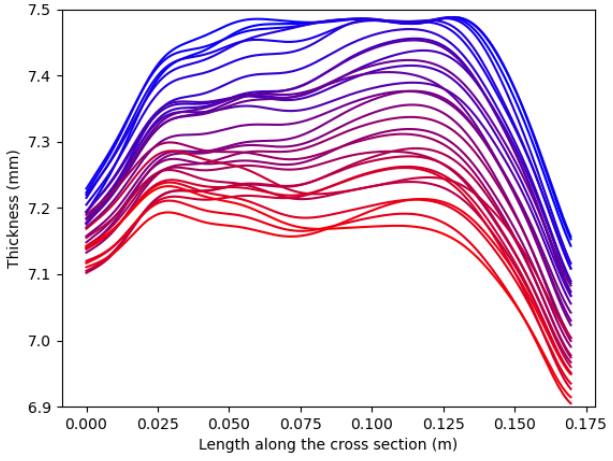

Figure 19: Cross sections of all absolute active tomography images computed during the erosion test.

Finally, in order to evaluate the potential bias due to the fact that dipersion curves are computed at ambient temperature instead of a temperature around 38°C, three cross sections are plotted in Figure 20:

- One corresponding to the data measured at the end of batch#3/day#2. The temperature of the structure was measured to be 39°C;
- A second corresponding to the data measured just before the erosion loop starts to batch#4/day#3. The temperature of the structure was measured to be 13°C;
- A third corresponding to the data measured just after the erosion loop starts to batch#4/day#3. The temperature of the structure was measured to be 37°C.

This allows to study the effect of temperature on absolute tomography without changing significantly the residual thickness of the structure. To do so, the first measure is performed at the end of the day, when the structure has a high temperature, the second after a night of cooling and without air flow and a third just after the structure has warmed up in the next batch, the erosion created during warm-up being relatively low. Those three states are plotted in Figure 20. What is very interesting is that despite a variation of several tens of degrees, during the night of cooling and then during the warm up, the maximum gap visible on the cross-sections is less than 0.1mm, meaning less than the theoretical precision of the method. Note finally that the small erosion created during warm-up is still visible on Figure 20 between the two red curves.

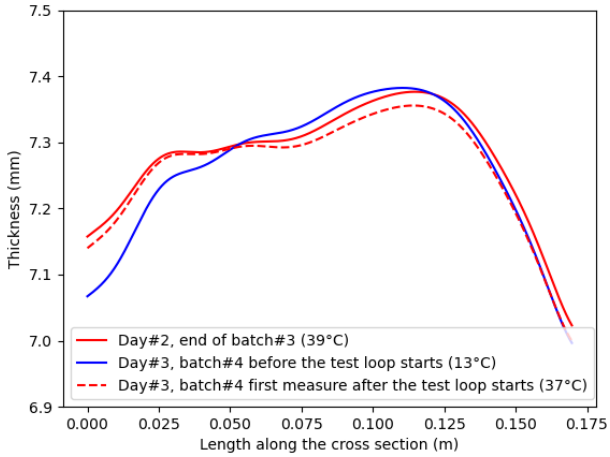

Figure 20: Comparison of cross sections at high and low temperature with the same rate of erosion.

To conclude this section, the autocalibration method seems to allow to compensate large variations of environmental conditions. It could be interesting to confirm this observation with more quantitative tests, for example in a climate chamber.

3.3.3. Passive tomography for absolute reconstructions

In this third subsection passive guided wave tomography is finally studied. Now that we demonstrated the interest of absolute tomography, passive tomography images of this pipe are computed in absolute mode.

The first image of absolute passive tomography is computed based on the signals measured just after the test started and is shown in Figure 21. As with absolute active tomography, the thickness background is not uniform whereas no erosion is created by the sand yet. Note however that the same pattern is obtained as with active data (Figure 17), comforting the idea that this is in reality the absolute healthy wall thickness of the pipe which is not constant because of the manufacturing process.

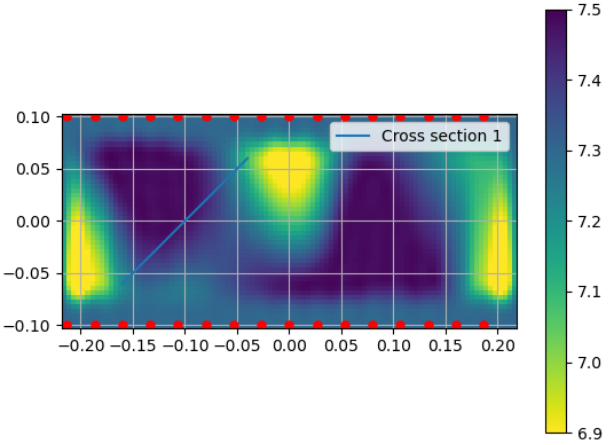

Figure 21: Absolute passive tomography computed at the start of the test. The colorbar is in millimeters and the axes are in meters.

Regarding the absolute passive tomography computed at the end of the test (see Figure 22), by comparing to Figure 21, it shows a reduction of thickness in the left part of the image as for the active case and the erosion shape and position are coherent with the air/sand flow path.

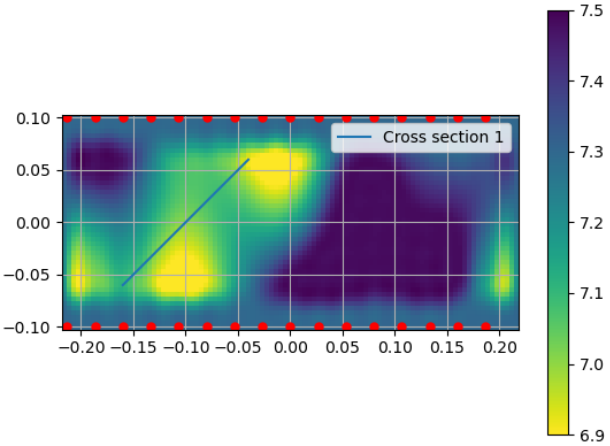

Figure 22: Absolute passive tomography computed at the end of the test. The colorbar is in millimeters and the axes are in meters.

Finally, to estimate the quality of thickness loss estimations of the passive tomography, cross sections are plotted in Figure 23. It shows a maximal thickness loss of 0.5mm which is a very good estimation compared to the punctual US

measurements that give 0.51mm +/- 0.1mm. We notice in Figure 23 that passive reconstructions are slightly less stable than active reconstructions. This is due to the fact that passive signals are imperfect approximations of active signals due to the limited acquisition time and thus contain a correlation residue making signals noisier in the bandwidth of interest. Knowing that, the passive tomography still gives a good estimation of the thickness losses due to the erosion by air/sand flow.

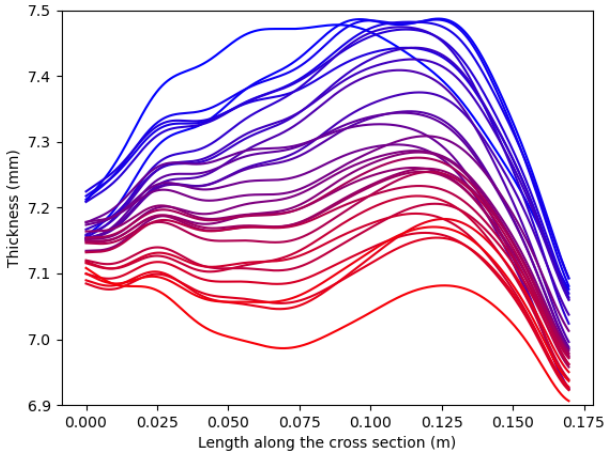

Figure 23: Cross sections of all absolute passive tomography images computed during the erosion test.

4. Conclusions

We have shown in this paper an application of passive guided wave tomography to a representative test case: a pipe instrumented in an accelerated air/sand erosion test loop. The noise from the test itself was used as our input data to reconstruct the evolution of the residual thickness of the instrumented part, this residual thickness evolving during the test.

We have seen that the ambient noise generated by the test loop disturbs active measurements even after several hundreds averages of the raw signals, whereas this same ambient noise is a source of information for passive reconstructions, without needing all the electronics to generate waves in the medium.

We then studied active tomography with a baseline. This study demonstrated that a baseline can become obsolete if it is not coherent with the EOC of the current state. For guided wave tomography it introduces a bias within the estimation of the thickness losses. For other guided waves based methods it can lead to very bad reconstructions if the changes in EOCs are not modeled correctly. This is one of the reasons why we prefer to work in absolute with the use of the autocalibration method instead of in relative to perform guided wave tomography in an SHM framework.

Absolute tomography was then studied with active and passive data. Both active and passive estimations of the residual thickness were coherent with reference punctual US measurements and considering a precision of 0.1mm to estimate thickness with guided wave tomography. One advantage of absolute tomography is that it is able to reconstruct the real absolute thickness whereas relative tomography assumes that the healthy thickness is the one corresponding to the nominal thickness given by the manufacturer. Knowing that, for pipes the tolerance on the thickness can reach 15% of the nominal thickness, tomography with a baseline can give a bad estimation of the residual thickness where absolute tomography approaches the exact estimate.

This paper also shows that absolute tomography seems, thanks to the autocalibration method, to compensate large variations of temperature (several tens of degrees). It could be interesting in future work to confirm this observation with tests in climate chamber.

Acknowledgments

We would like to thank Cybernetix from Technip Energies for its collaboration, and DNV Høvik for its help in using the erosion loop.

References

[1] M.J.S Lowe, D.N. Alleyne and P. Cawley, Defect detection in pipes using guided waves, *Ultrasonics*, vol.36, pp.147-154, 1998.

[2] A. Delory, F. Lemoult, A. Eddi and C. Prada, Guided elastic waves in a highly-stretched soft plate, *Extreme Mechanics Letters*, pp.102018, 2023.

[3] Z. Qian, C. Zhang, P. Li, B. Wang, Z. Qian, I. Kuznetsova and X.-Y. Li, A dictionary reconstruction approach for separating helical-guided waves in cylindrical pipes, *Journal of Physics D: Applied Physics*, 2023.

[4] H. W. Kim, H. J. Lee and Y. Y. Kim, Health monitoring of axially-cracked pipes by using helically propagating shear-horizontal waves, *NDT & E International*, vol.46, pp.115-121, 2012.

[5] P. W. Loveday, C. S. Long and D. A. Ramatlo, Ultrasonic guided wave monitoring of an operational rail track, *Structural Health Monitoring*, vol 19, pp.1666-1684, 2020.

[6] P. Huthwaite and F. Simonetti, High-resolution guided wave tomography, *Wave Motion*, vol.50, pp.979-993, 2013.

[7] A. A. E. Zimmermann, Shear-horizontal guided wave tomography, *Imperial College London*, 2022.

[8] T. Druet, J.-L. Tastet, B. Chapuis and E. Moulin, Autocalibration method for guided wave tomography with undersampled data, *Wave Motion*, vol.89, pp.265-283, 2019.

[9] C. Liu, J. B. Harley, M. Bergés, D. W. Greve and I. J. Oppenheim, Robust ultrasonic damage detection under complex environmental conditions using singular value decomposition, *Ultrasonics*, vol.58, pp.75-86, 2015.

[10] K. Sabra, A. Srivastava, F. Lanza di Scalea, I. Bartoli, P. Rizzo and S. Conti, Structural health monitoring by

extraction of coherent guided waves from diffuse fields, *Journal of the Acoustical Society of America*, vol.132, pp.8-13, 2008.

[11] O. Lobkis and R. Weaver, On the emergence of the Green's function in the correlations of a diffuse field, *Journal of the Acoustical Society of America*, vol.6, pp.3011-3017, 2001.

[12] T. Druet, A. Recoquillay, B. Chapuis and E. Moulin, Passive guided wave tomography for structural health monitoring, *The Journal of the Acoustical Society of America*, vol.146, pp.2395-2403, 2019.

[13] A. Recoquillay, T. Druet, S. Nehr, M. Horpin, O. Mesnil, B. Chapuis and O. d'Almeida, Guided wave imaging of composite plates using passive acquisitions by fiber Bragg gratings, *The Journal of the Acoustical Society of America*, vol.147, pp.3565-3574, 2020.

[14] T. Druet, B. Chapuis, M. Jules, G. Laffont and E. Moulin, Passive guided waves measurements using fiber Bragg gratings sensors, *The Journal of the Acoustical Society of America*, vol.144, pp.1198–1202, 2018.

[15] T. Druet, H. T. Hoang, S. Nehr, G. Laffont and B. Chapuis, Effect of Fiber Bragg Gratings Receivers' Directivity on Guided Wave Tomography of Pipe, in *The 12th International Workshop on Structural Health Monitoring*, 2019.